# Impact of tropical biomass burning emissions on the diurnal cycle of upper tropospheric CO 2 retrieved from NOAA 10 satellite observations

A. Chedin, S. Serrar, N.A. Scott, C. Pierangelo, Philippe Ciais

▶ **To cite this version:**

A. Chedin, S. Serrar, N.A. Scott, C. Pierangelo, Philippe Ciais. Impact of tropical biomass burning emissions on the diurnal cycle of upper tropospheric CO 2 retrieved from NOAA 10 satellite observations. Journal of Geophysical Research, 2005, 110 (D11), 10.1029/2004JD005540 . hal-02924615

**HAL Id: hal-02924615**
**https://hal.science/hal-02924615v1**

Submitted on 17 Sep 2020

**HAL** is a multi-disciplinary open access archive for the deposit and dissemination of scientific research documents, whether they are published or not. The documents may come from teaching and research institutions in France or abroad, or from public or private research centers.

L'archive ouverte pluridisciplinaire **HAL**, est destinée au dépôt et à la diffusion de documents scientifiques de niveau recherche, publiés ou non, émanant des établissements d'enseignement et de recherche français ou étrangers, des laboratoires publics ou privés.

# Impact of tropical biomass burning emissions on the diurnal cycle of upper tropospheric $CO_2$ retrieved from NOAA 10 satellite observations

A. Chédin,[1] S. Serrar,[1,2] N. A. Scott,[1] C. Pierangelo,[1] and P. Ciais[2]

Received 22 October 2004; revised 2 February 2005; accepted 14 March 2005; published 14 June 2005.

[1] Four years (July 1987 to June 1991) of monthly mean upper tropospheric $CO_2$ mixing ratios over the tropics are retrieved from the observations, at 0730 LT (day) and 1930 LT (night) local time, of the meteorological satellite NOAA 10. Analysis of night minus day differences (N-DD) shows large diurnal variations of $CO_2$, of the order of 2–3 ppm, during months and over regions affected by biomass burning. The patterns of these diurnal variations are in very good agreement with the diurnal and seasonal variations of biomass burning activity. We interpret them as the signal of $CO_2$ plumes being rapidly uplifted by fire-induced convection into the upper troposphere during the daytime peak of fire activity and then being rapidly dispersed at night by large-scale atmospheric transport. The upper air $CO_2$ diurnal cycle closely follows the seasonal distribution of burned areas from the European Space Agency's monthly Global Burnt Scar satellite product, which is recognized as yielding reasonable estimates of burned areas for large and presumably intense fires. The largest N-DD values are found in 1990 over southern Africa in agreement with the reported interannual variability of fire activity. However, the magnitude of these extreme signatures, on the order of 5 ppm locally, is larger than what can reasonably be expected from either in situ observations or from simulations, suggesting some contamination of the N-DD retrieval by fire emission products other than $CO_2$. It is concluded from a detailed sensitivity analysis that the presence of high-altitude and large optical depth aerosols, or of elevated tropospheric ozone concentrations, as are often encountered in fire plumes, may significantly contaminate the retrieved $CO_2$ signal (by up to 2–3 ppm for extreme events). The possible contaminating effects of undetected fire-induced thin cirrus (optical depths less than 0.05 at 14 μm) are also quantified.

**Citation:** Chédin, A., S. Serrar, N. A. Scott, C. Pierangelo, and P. Ciais (2005), Impact of tropical biomass burning emissions on the diurnal cycle of upper tropospheric $CO_2$ retrieved from NOAA 10 satellite observations, *J. Geophys. Res.*, *110*, D11309, doi:10.1029/2004JD005540.

## 1. Introduction

[2] Biomass burning is an important source of atmospheric $CO_2$, aerosols, and chemically important gases. It is as important to global chemistry as industrial activities in the developed world [*Crutzen and Andreae*, 1990]. Biomass burning is a key component of the global carbon budget, currently releasing 2.6 pg C from fires in the tropical and subtropical ecosystems (an estimation from *van der Werf et al.* [2003]) to the atmosphere each year, most of it (~90%) being emitted in the form of carbon dioxide, although there is important spread among various estimates. For example, *Hoelzemann et al.* [2004], using the new global wildland fire emission model (GWEM) based on the Global Burnt Scar (GLOBSCAR) burned area satellite data [*Simon et al.*, 2004] and the Moderate Resolution Imaging Spectroradiometer (MODIS) land cover map, reevaluated the emission totals for the year 2000 at 1.74 pg C, a value significantly smaller than other previous estimates but still considerable [see also *Kasischke and Penner*, 2004].

[3] Within the tropics, savanna fires alone are estimated to contribute 22% of the biomass burned globally [*Andreae*, 1996], with two thirds of savanna fire emissions occurring in Africa [*Hao and Liu*, 1994]. The carbon released by savanna fires is a seasonal source of $CO_2$ to the atmosphere, whereas (at steady state) an equivalent amount of atmospheric $CO_2$ is reincorporated into the vegetation during the wet growing season. In contrast, carbon released by the combustion of tropical forests, in particular by infrequent fires affecting moist forests with peat soils [*Siegert et al.*, 2001], is a net source durably added to the atmosphere. Simulations of the impact of biomass burning on the

[1] Laboratoire de Météorologie Dynamique, l'Institut Pierre-Simon Laplace, Ecole Polytechnique, Palaiseau, France.
[2] Laboratoire des Sciences du Climat et de l'Environnement, Commissariat à l'Energie Atomique/l'Institut Pierre-Simon Laplace, Gif-sur-Yvette, France.

Copyright 2005 by the American Geophysical Union.
0148-0227/05/2004JD005540

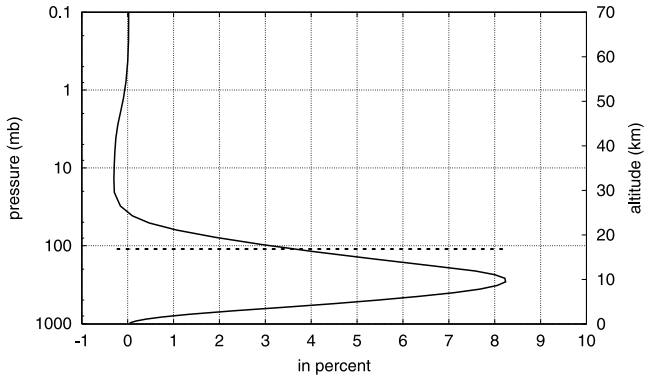


**Figure 1.** Mean normalized $CO_2$ Jacobian (partial derivative of the TIROS-N Operational Vertical Sounder observations with respect to $CO_2$ variations) of the High-Resolution Infrared Sounder $CO_2$ sensitive channels (in %). Dashed line indicates mean tropical tropopause level.

atmospheric $CO_2$ distribution using atmospheric transport models suggest a moderate effect of fires on the $CO_2$ seasonal cycle [*Wittenberg et al.*, 1998; *van der Werf et al.*, 2004] but a large impact on the interannual variability in growth rates [*Langenfelds et al.*, 2002; *van der Werf et al.*, 2004]. Biomass burning as a source of $CO_2$ is generally not explicitly accounted for in atmospheric inversions of $CO_2$ sources and sinks, although recent studies suggested that it could be a key contributor of the $CO_2$ interannual variability [*Schimel and Baker*, 2002; *Langenfelds et al.*, 2002; *Rodenbeck et al.*, 2003].

[4] Biomass burning occurs in Africa, South America, and Indonesia during the dry season of each hemisphere. During the fires, chemical compounds are released and are sometimes uplifted at altitudes of several kilometers [*Lavoué et al.*, 2000; *Andreae et al.*, 2004] and are then transported over long distances [*Hauglustaine et al.*, 1998; *Andreae et al.*, 2001; *Stohl et al.*, 2002; *Chatfield et al.*, 2002]. Better understanding of the role of vegetation burning emissions on atmospheric chemistry has been obtained from regional campaigns, ground-based and aircraft measurements from specific sites, such as the Southern Africa Fire-Atmosphere Research Initiative (SAFARI) [*Lindesay et al.*, 1996], the Transport and Atmospheric Chemistry Near the Equator—Atlantic (TRACE-A) [*Fishman et al.*, 1996], or the Experiment for Regional Sources and Sinks of Oxidants (EXPRESSO) [*Delmas et al.*, 1999]. Unfortunately, $CO_2$ was not measured systematically during these campaigns.

[5] Recent progress in trace gas satellite remote sensing offers a way to complement in situ studies by adding extensive spatial and temporal coverage. This is the case, for example, for instruments like the interferometric monitor for greenhouse gases that flew on the Japanese ADEOS platform in 1996 or the Measurement of Pollution in the Troposphere (MOPITT) instrument now flying on board the NASA/Terra platform among others.

[6] Recently, *Chédin et al.* [2003] showed that upper air $CO_2$ concentration can be retrieved from observations of the Television Infrared Operational Satellite–Next Generation (TIROS-N) Operational Vertical Sounder (TOVS), whose main mission is to measure atmospheric temperature and moisture at global scale. Flying aboard the NOAA polar meteorological satellites since 1978 [*Smith et al.*, 1979], this instrument consists of the High-Resolution Infrared Sounder (HIRS 2), the microwave sounding unit (MSU), and the stratospheric sounding unit. In the 15 and 4.3 μm spectral bands, HIRS 2 radiances mostly depend on the temperature of the atmosphere but also, although weakly [*Chédin et al.*, 2002], on the $CO_2$ concentration and on the concentrations of other greenhouse gases (as $O_3$ around 15 μm or $N_2O$ and CO around 4.3 μm). Also sensitive to the temperature of the atmosphere, the observations made simultaneously by MSU are not sensitive to $CO_2$ (or to the above greenhouse gas concentrations). This allows the two signals to be separated. Figure 1 shows that the mean normalized $CO_2$ Jacobian (partial derivative of the satellite observations with respect to atmospheric layer $CO_2$ variations) of the HIRS 2 $CO_2$ sensitive channels exhibits maximum sensitivity at around 200 hPa.

[7] The approach developed by *Chédin et al.* [2003], consisting of a nonlinear regression inverse radiative transfer model based on the multilayer perceptron [*Rumelhart et al.*, 1986], was applied to NOAA 10 observations, between July 1987 and June 1991, in the tropical zone (20°N–20°S). This choice was dictated by (1) the much greater stability of the temperature vertical structure, resulting in a better separation of the $CO_2$ and temperature signals; (2) the fact that space retrieved $CO_2$ columns are of major interest in a region where the surface flask network is sparse and has no coverage over the continents; and (3) the fact that strong convective mixing rapidly transmits the signal of $CO_2$ surface fluxes to that part of the troposphere observed by the satellite, making upper air $CO_2$ data useful to constrain sources in inversions [*Houweling et al.*, 2003]. In good agreement with accurate upper tropospheric in situ measurements made on board commercial aircrafts over the western Pacific between 1993 and 1999 [*Matsueda et al.*, 2002], HIRS 2 retrieved $CO_2$ concentrations made it possible to describe seasonal and year-to-year fluctuations of $CO_2$ in the upper troposphere. These interannual variations confirmed the correlation between the $CO_2$ growth rate and the Southern Oscillation index during the declining 1986–1987 El Niño, the strong 1988–1989 La Niña, and the beginning of the 1991 El Niño.

[8] Being Sun-synchronous, NOAA 10 observes the tropics at 0730 LT (daytime) and 1930 LT (nighttime), opening the way to the study of the diurnal variations of $CO_2$ within the middle to upper troposphere. To do so, the approach described by *Chédin et al.* [2003], formerly limited to the processing of nighttime observations, was here enhanced to process daytime observations as well. The main modifications brought to the retrieval method as well as other significant improvements aiming at increasing its precision are summarized in section 2, which also shows the resulting upper troposphere $CO_2$ concentration "nighttime minus daytime retrieval difference," hereinafter referred to as the N-DD signal. In section 3, after having summarized what is presently known of the seasonal and diurnal variability of tropical vegetation fires, we show that there is a striking correlation between the N-DD signal and independent indicators of biomass burning activity. An interpretation of the N-DD signal variability is then

presented in section 4 and is discussed in section 5. Section 6 presents our conclusions.

## 2. Retrieving $CO_2$ Diurnal Variations From TOVS

### 2.1. Retrieval Algorithm Improvement

[9] To allow the processing of daytime as well as nighttime observations, the retrieval method described by *Chédin et al.* [2003] has been modified by removing from the predictors the HIRS 2 window channel 18 measuring at 4.0 μm, a channel potentially contaminated by solar radiation. The regression predictors are now the five HIRS 2 channels 2–6 measuring at 15 μm, sensitive to both $CO_2$ and atmospheric temperature, and the two MSU microwave channels 3 and 4, only sensitive to temperature. In any case, training of the multilayer perceptron is performed using the Thermodynamic Initial Guess Retrieval (TIGR) climatological data set [*Chédin et al.*, 1985; *Chevallier et al.*, 1998].

[10] We made two other improvements to the original method. First, an improved radiative transfer model bias removal procedure was designed, relying on comparisons between satellite observations and their simulations by the radiation model fed not only with collocated radiosondes but also with collocated operational meteorological analyses from the European Centre for Medium-Range Weather Forecasts. This has resulted in a greater smoothness and latitudinal continuity of the adjustment factors, compared to the results of *Chédin et al.* [2003]. Second, we reevaluated the noises affecting the observed radiances (instrumental noise) as well as the simulated radiances (forward radiative transfer model noises) used to train the regressions. In particular, values of new model noises, previously ranging from 0.08 to 0.10 K according to the channel considered, were shown as being underestimated and have now been fixed on the basis of numerous trials at a constant, channel-independent value of 0.15 K. This modification has resulted in a significantly reduced range of variation of the spatial distribution of $CO_2$ as compared to the results of *Chédin et al.* [2003]. This is confirmed by comparing, for example, the retrieved $CO_2$ 4-year mean seasonal cycle peak-to-peak difference for the latitude band 20°–15°N (where it is the largest): 4.6 ppm now, 4.8 ppm as measured by *Matsueda et al.* [2002], and formerly 6.7 ppm as measured by *Chédin et al.* [2003].

### 2.2. Diurnal Variation of Upper Tropospheric $CO_2$ Concentration

[11] Four years of NOAA 10 observations at 0730 and 1930 LT, from July 1987 to June 1991, have been interpreted in terms of upper tropospheric $CO_2$ column. Individual cloud-free daily retrievals at a spatial resolution of $1° \times 1°$ are binned into monthly maps at a spatial resolution of $15° \times 15°$ at 0730 and at 1930 LT over the latitude band 20°N–20°S.

[12] For each month we compute the difference in column-averaged upper tropospheric $CO_2$ between 1930 and 0730 LT by averaging daily differences. For each $15° \times 15°$ grid box a day is retained if clear-sky situations are available for both afternoon and morning satellite passes. On a monthly basis, at least 100 such daily differences are required within each 15° grid box to produce one monthly N-DD difference item. This threshold accounts for the prevalence of clouds over the tropics and explains (white) areas with no data in Figures 2–5 presented below.

[13] In Figure 2, monthly N-DD values have been lumped into seasons and have been averaged over the 4 years considered. Contrary to our expectation of relatively smooth and weak upper troposphere $CO_2$ diurnal variations, the N-DD shows regional maxima of up to 3 ppm during June, July, and August over southern Africa and southern America and of ~2 ppm during December, January, and February over northern Africa (south Asia being obscured by persistent cloudiness), i.e., during the dry winter of each hemisphere. On a monthly basis (see Figures 3–5), again averaged over the 4 years, a weaker regional enhancement of N-DD can be seen during February over northern Africa and during September over southern Africa and southern America.

[14] We performed a statistical analysis of the variability in N-DD daily retrievals over land. This resulted in mean monthly standard deviation (averaged, month by month, over the 4 years) of the order of 1 ppm (see Figure 6), a value well below the 3 ppm mean spatial gradients in N-DD observed in Figures 3–5, with negligible temporal variations.

## 3. Relationship Between Upper Tropospheric $CO_2$ Diurnal Variations and Biomass Burning Activity

### 3.1. Seasonal and Diurnal Variations of Fire Emissions in the Tropics

[15] Accurate quantification of the amounts and impacts of trace gases and particulate matter emitted from biomass burning on a regional and global basis has gained the attention of the atmospheric chemistry modeling community since the 1980s [*Seiler and Crutzen*, 1980]. Such quantification requires an accurate knowledge of the spatial and temporal distribution of fires. Over the past decades, major improvements in the ability to detect and map fires using a number of different satellite systems have been achieved. Several studies have used different remotely sensed data (e.g., advanced very high resolution radiometer (AVHRR), Along Track Scanning Radiometer (ATSR), Geostationary Operational Environmental Satellite (GOES), or Tropical Rainfall Measuring Mission (TRMM)) and techniques to detect either active fires [*Cahoon et al.*, 1992; *Prins and Menzel*, 1992; *Arino and Mellinotte*, 1995; *Giglio et al.*, 2003] or burned areas [*Barbosa et al.*, 1997; *Simon et al.*, 2004].

[16] These studies made it possible to assemble fire emission inventories [*Barbosa et al.*, 1999; *Duncan et al.*, 2003; *Schultz*, 2002; *van der Werf et al.*, 2003], though often incomplete or of unequal quality on the global scale. Despite those recent improvements, quantifying fire emissions across large spatial scales still suffers from large uncertainties, mainly due to uncertainties in fuel loads, combustion completeness, and burned area [*Hoelzemann et al.*, 2004].

[17] Fire activity is seasonal, generally lasting 3–4 months, with the burning season being longer in the Southern Hemisphere [*Duncan et al.*, 2003]. Global fire emissions seasonality has recently been analyzed in detail by *Hoelzemann et al.* [2004]. These authors compared

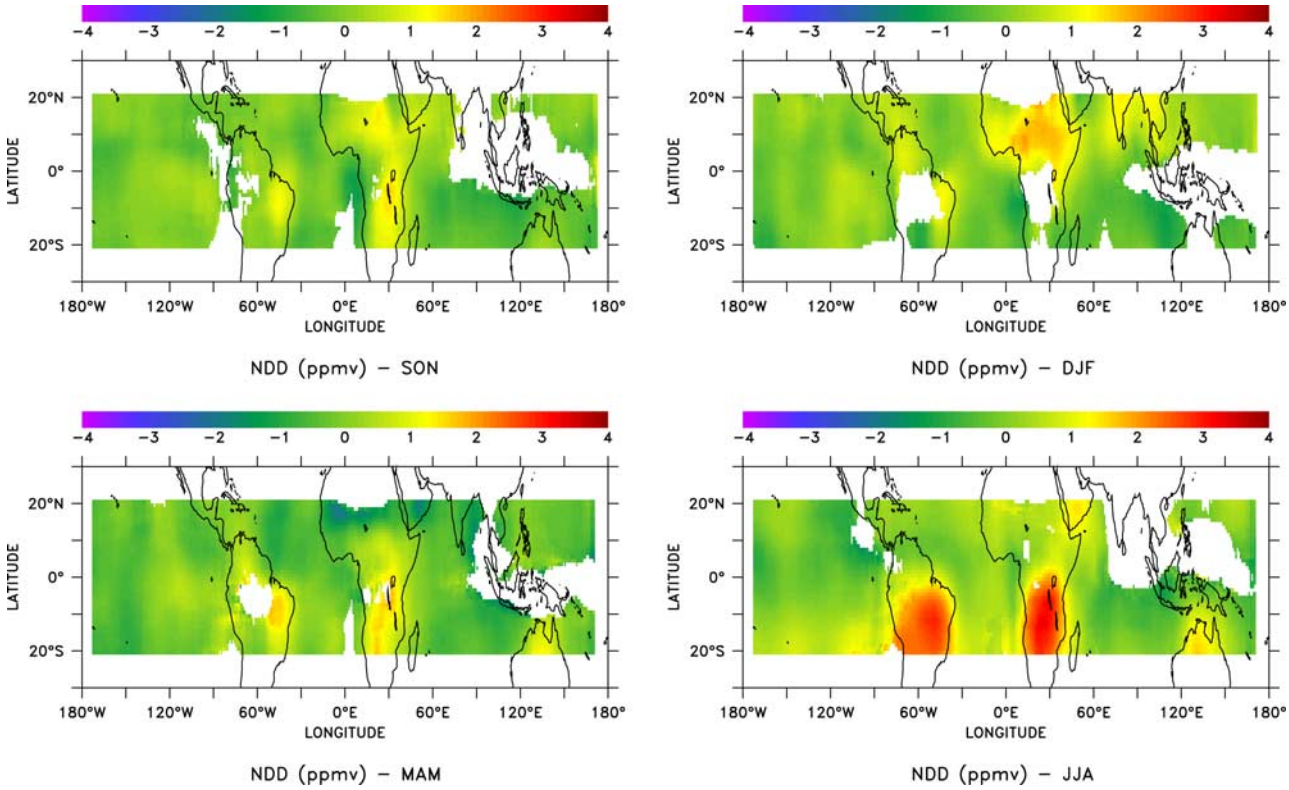


**Figure 2.** Seasonal mean difference between 1930 and 0730 LT of mean upper tropospheric mixing ratios of $CO_2$ over the tropics (20°N–20°S) averaged over the period July 1987 to June 1991. Spatial resolution is 15° × 15°, 1° by 1° moving average.

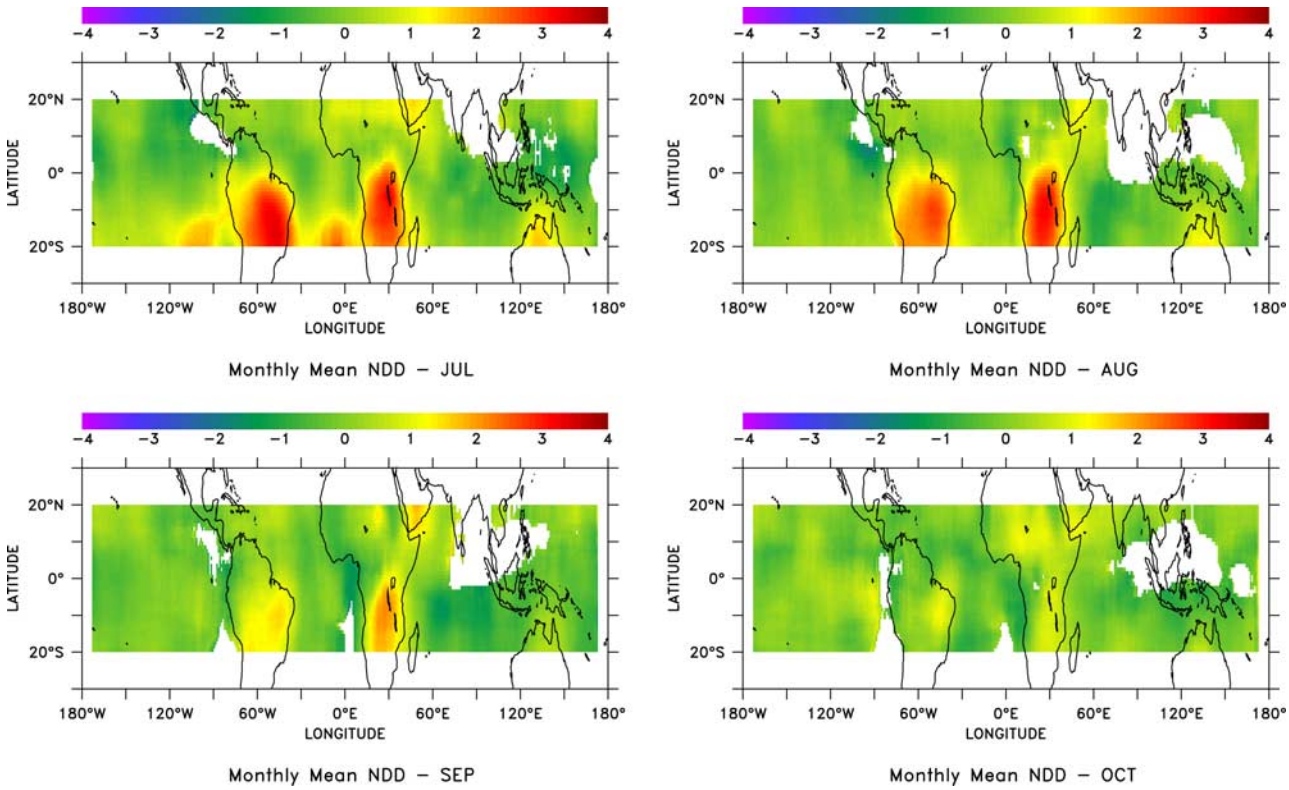


**Figure 3.** Monthly mean difference between 1930 and 0730 LT of mean upper tropospheric mixing ratios of $CO_2$ over the tropics (20°N–20°S) averaged over the period July 1987 to June 1991. Spatial resolution is 15° × 15°, 1° by 1° moving average. Months are July to October.

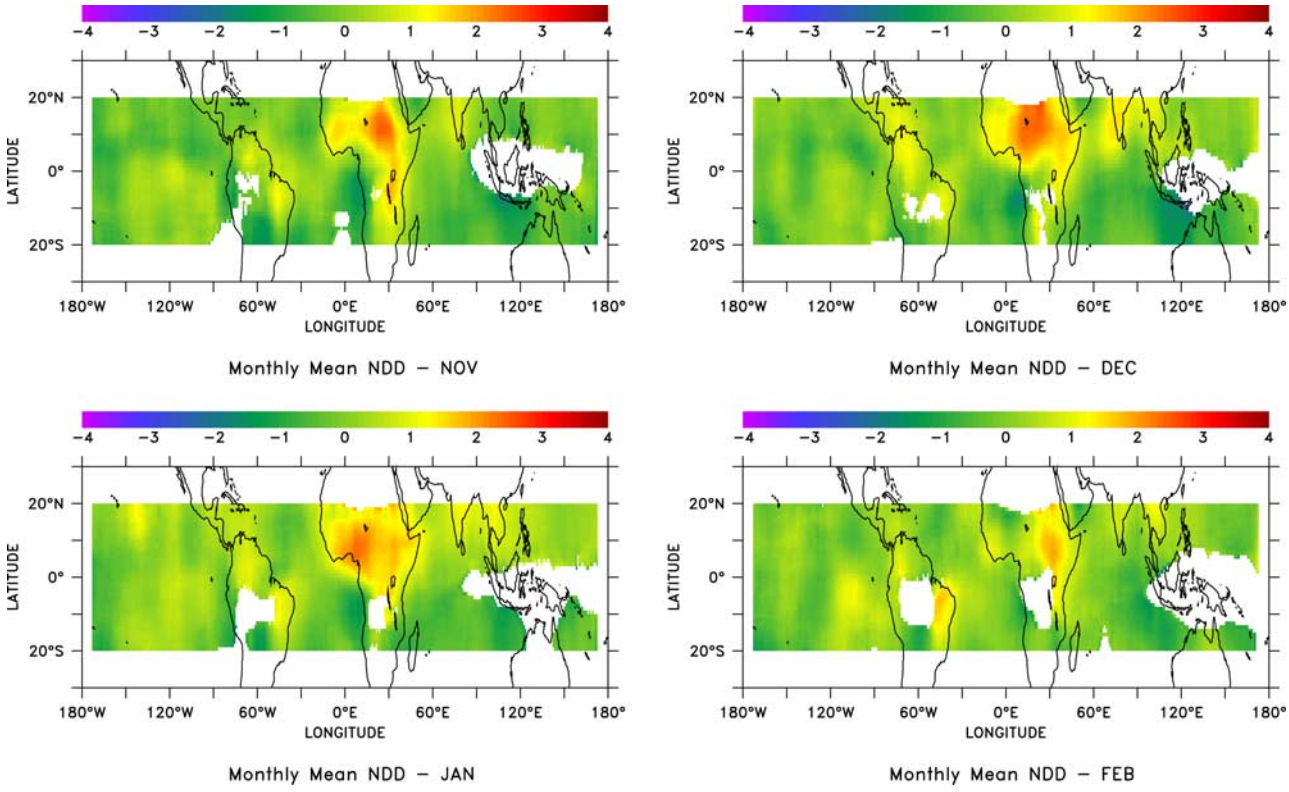


**Figure 4.** Same as Figure 3 but for the months November to February.

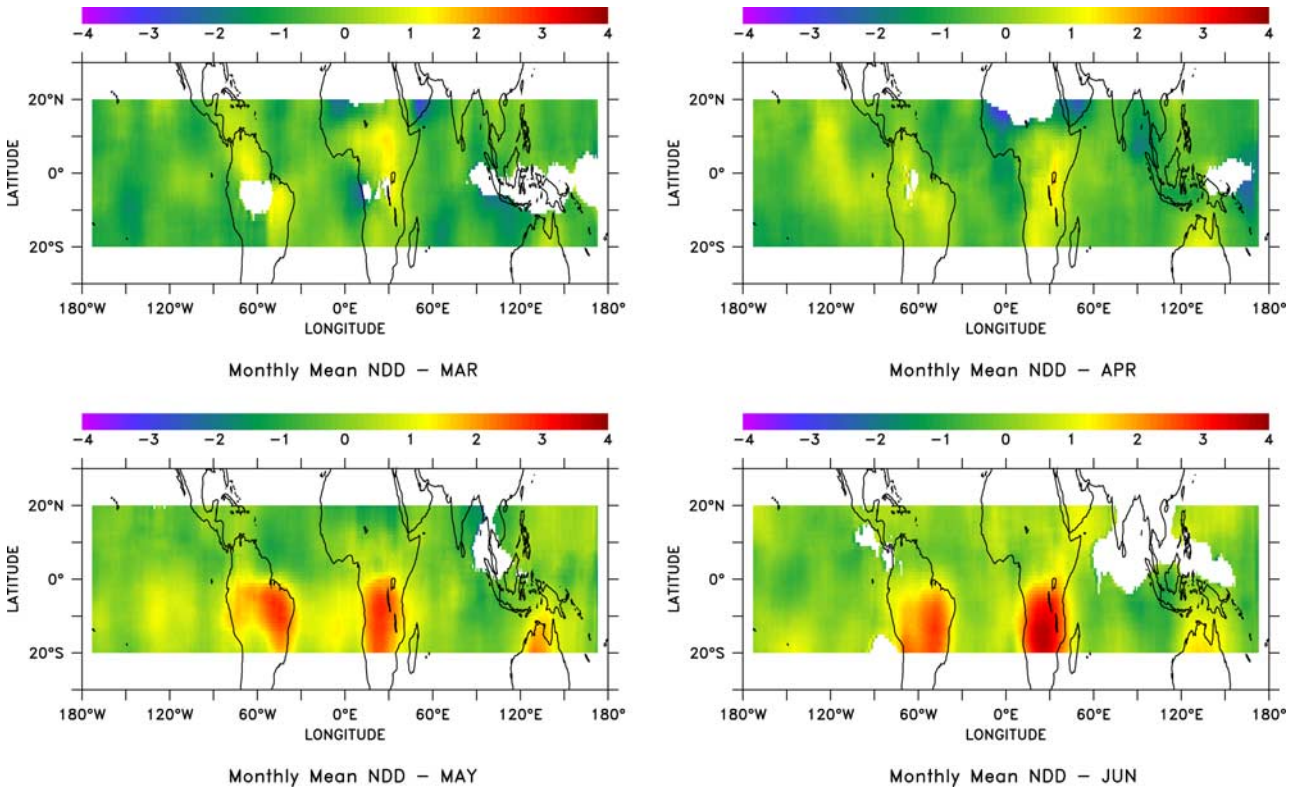


**Figure 5.** Same as Figure 3 but for the months March to June.

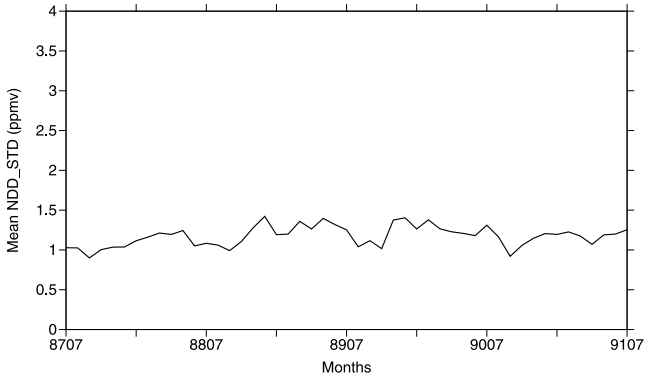


**Figure 6.** Four-year averaged monthly mean standard deviation (in ppm) of the daily N-DD retrievals sample over land (Africa and South America).

monthly number of areas burned from the GLOBSCAR product [*Simon et al.*, 2004] to ATSR active fire counts product [*Arino and Plummer*, 2001] for the year 2000 and showed that for GLOBSCAR the maxima occur in June and December, while for ATSR the maxima are observed in August and December. According to *Hoelzemann et al.* [2004, p. 13] such discrepancies can be reconciled because "active fire counts do not reveal information about the associated burnt scar size. Maximum of the ATSR active fire counts in August results from many small fires with small burnt scars, while the GLOBSCAR peak in June takes place because of a reduced number of larger fires." In southern Africa, results from GWEM indicate that the fire season extends from April to October and shows a peak in June; in northern Africa the fire season extends from November to April, reaching its maximum in December. A much smaller contribution is found for South America, with a peak in August for southern South America and in January for northern South America [*Hoelzemann et al.*, 2004]. GWEM results are in agreement with the seasonality of biomass burning in Africa as described by *Cahoon et al.* [1992] and *Cooke et al.* [1996] and with results on burned area from *Barbosa et al.* [1999]. As for fire seasonality in South America, GWEM results seem to be in agreement with *van der Werf et al.* [2003] and *Duncan et al.* [2003] except for northern South America where GLOBSCAR show 1–2 months advance.

[18] Fire activity generally undergoes a strong diurnal cycle. Using GOES 8 observations, *Prins et al.* [1998] report that through the 1995 burning season in South America a diurnal signature is clearly evident with peak burning occurring in the early afternoon to midafternoon local time. The number of fire pixels observed at this time is typically 2–3 times greater than observed 3 hours earlier or later and nearly 7 times greater than observed 6 hours earlier. Similar results are reported by *Hsu et al.* [1996]. The existence of a strong diurnal cycle of African savanna fires is also reported by *Langaas* [1993], using field observations and thermal satellite images.

### 3.2. N-DD and Biomass Burning Activity

[19] The seasonality of the N-DD maxima in Figures 3–5 follows that of fire activity, indicating that above burning areas, there is an important excess of $CO_2$ in the upper troposphere at 1930 LT, several hours after the daily peak burning, compared to 0730 LT. Seasonal changes in the location of the N-DD maxima within the year compare well with emission maps derived by *Duncan et al.* [2003] from aerosol indexes or ATSR fire counts or by *van der Werf et al.* [2003] from TRMM fire counts (see Figures 2 and 7), keeping in mind that the periods analyzed are different and that the N-DD is a middle to upper tropospheric signal whereas TRMM fire counts describe a surface product.

[20] In northern Africa, fire activity starts first in the interior of the sub-Saharan region (Sudan, Chad, and Ethiopia) by September-October and spreads to the west and south by December in agreement with fire seasonality results from GLOBSCAR (see, e.g., http://shark1.esrin.esa.it/ionia/FIRE/BS/ATSR/docs/World_Summit_Fire.ppt, August 2002). In southern Africa, *Cahoon et al.* [1992] have described a west-to-east displacement in vegetation fires between March and November due to drier conditions spreading from Namibia to the east. The evolution of the N-DD maxima shown in Figures 3–5 illustrates the description made by *Cahoon et al.* [1992] well. In May, burning activity is widespread in the west and the interior of southern Africa. In June, burning is at its peak in the southern part of the Democratic Republic of Congo. From July to October the fires spread to the east and wane in some western and interior nations. Fire activity continues along the east coast of Africa (Kenya and Tanzania) up to November but ceases in December. As for northern Africa the evolution of the N-DD maxima in southern Africa is in good agreement with the GLOBSCAR burned areas product. In southern Africa the N-DD is in agreement with the emissions derived by *van der Werf et al.* [2003], although in advance by roughly 1 month (Figure 8). It is worth pointing out that there is no conflict between our results and observations from the SAFARI experiment identifying the peak of burning in July and August: The eastern part of Africa (South Africa and Mozambique) measured during SAFARI is affected by fires 2 months after the western part [*Simon et al.*, 2004].

[21] In South America the N-DD enhancement south of the equator begins in May and culminates in July and August. Emission inventories from *van der Werf et al.* [2003] depict scattered fires with low-intensity emissions in this region in May (Figure 7) but show a main peak in burning activity in August-September [see also *Duncan et al.*, 2003], that is, 1 month later than the N-DD regional maximum. This discrepancy could be caused by the fact that different periods were analyzed, by shortcomings in emission maps derived from fire counts, or by the fact that the N-DD is more sensitive to fewer large fires than to numerous smaller fires. In agreement with *van der Werf et al.* [2003] and *Duncan et al.* [2003], however, the N-DD shows a small area of enhancement near the mouth of the Amazon River which continues through December while the majority of burning in Brazil dwindles by October. The seasonality of fires in Columbia and Venezuela (December to April) is also observed in the N-DD maps. More generally, N-DD maxima for northern South America occur in December-January in agreement with *Hoelzemann et al.* [2004] but earlier than *van der Werf et al.* [2003] and *Duncan et al.* [2003].

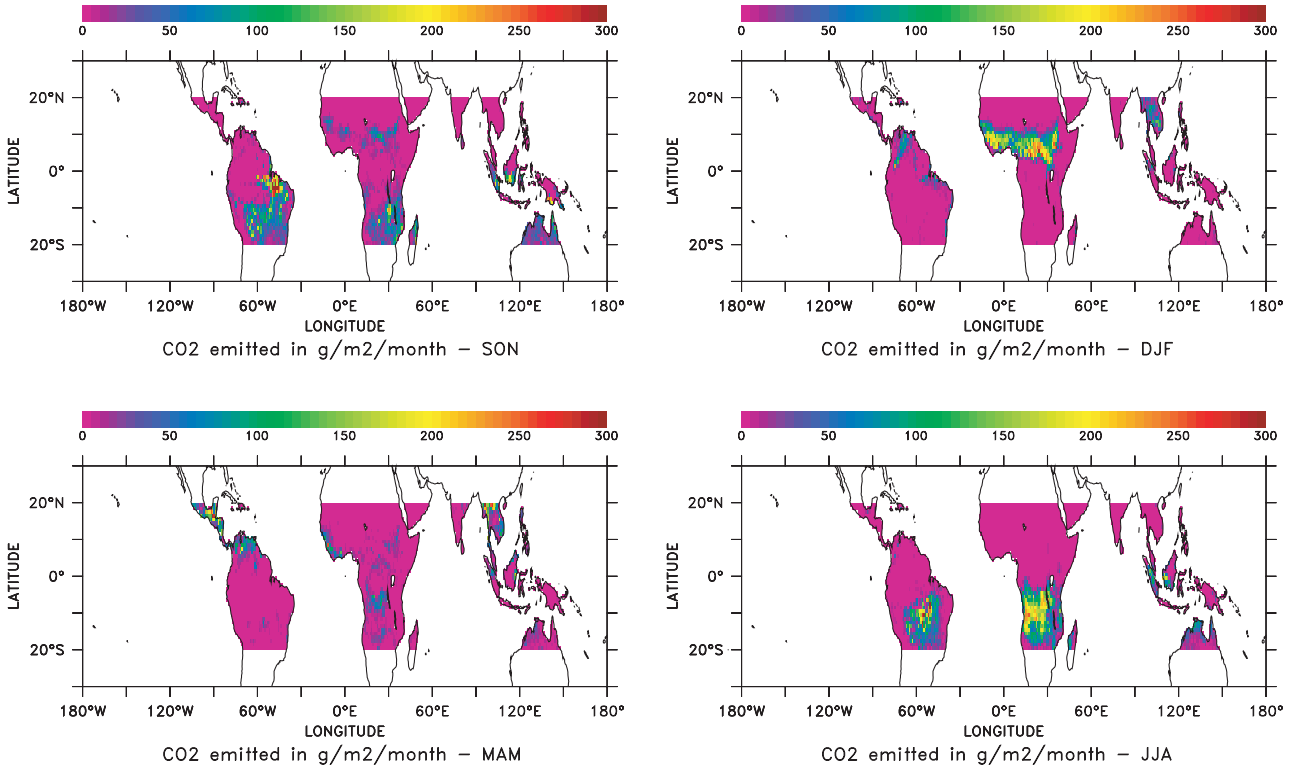


**Figure 7.** Seasonal mean fire emissions of carbon dioxide in g $m^{-2}$ $month^{-1}$ from *van der Werf et al.* [2003] averaged over the period 1997–2002. See also http://www.gps.caltech.edu/~jimr/randerson.html.

[22] The N-DD also exhibits interannual variability. Figure 8 shows the time series of the monthly mean N-DD averaged over land (left axis) in northern Africa, 0°–15°N (thick dashed line), and in southern Africa, 0°–20°S (thick solid line). As expected, the two time series are opposite in phase as are the burning dry seasons in each hemisphere. Also plotted in Figure 8 is the 1997–2002 averaged time series of the carbon dioxide fire emissions (in g $m^{-2}$ $month^{-1}$, right axis) from *van der Werf et al.* [2003], repeated 4 times for comparison (thin dashed line is 0°–20°S, and thin solid line is 0°–15°N). The maxima of N-DD occur in June over southern Africa and in December over northern Africa in better agreement with the emissions of *Hoelzemann et al.* [2004] based on GLOBSCAR burned areas than with those of *Duncan et al.* [2003] based on ATSR fire counts. This suggests that the seasonal changes in N-DD are more in phase with burned area than with fire counts seasonal changes and, consequently, that the N-DD relates more directly to the burned scar size than to the number of fires. Figure 8 also suggests that the emissions over southern Africa were higher in 1989–1990 than in 1987–1988, consistent with the results of *Barbosa et al.* [1999].

[23] A similar behavior of the N-DD is observed for Central and South America. Figure 9 shows the N-DD time series for the two regions: 0°–10°N (dashed line) and 0°–15°S (solid line). As expected, the N-DD maxima for 0°–10°N are much lower than over Africa or southern South America, indicating a less intense fire activity. Maxima for southern South America occur in June-July, 1 month earlier than found by *van der Werf et al.* [2003] and *Duncan et al.* [2003] and also by *Hoelzemann et al.* [2004] for year 2000.

[24] The N-DD signal, based upon measurements of the concentration of $CO_2$ twice a day, is better adapted to depicting the seasonality of fires than the retrieved column $CO_2$ concentrations themselves. Over southern Africa (0°–20°S), for example, the variations of $CO_2$ retrieved from TOVS (Figure 10b) appear much less correlated with fires

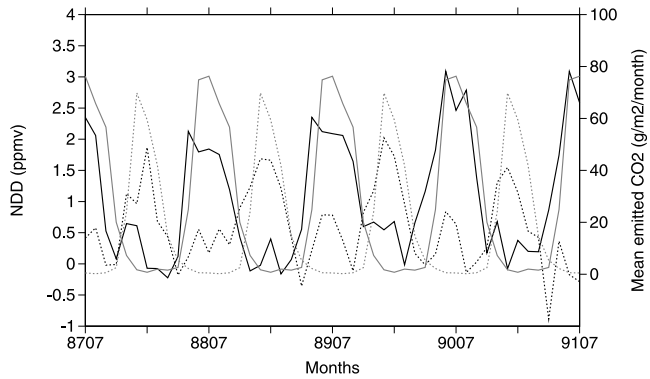


**Figure 8.** Time series of the monthly mean N-DD (in ppm, left axis) averaged over land for two regions: thick dashed line for northern Africa (0°–15°N) and thick solid line for southern Africa (0°–20°S). Averaged time series for 1997–2002 of the carbon dioxide fire emissions (in g $m^{-2}$ $month^{-1}$, right axis) from *van der Werf et al.* [2003] is repeated 4 times for comparison; light dashed line is for 0°–20°S, and light solid line is for 0°–15°N. Consistent with estimations of *Barbosa et al.* [1999], N-DD suggests much higher emissions over southern Africa in 1989–1990 than, for example, in 1987–1988.

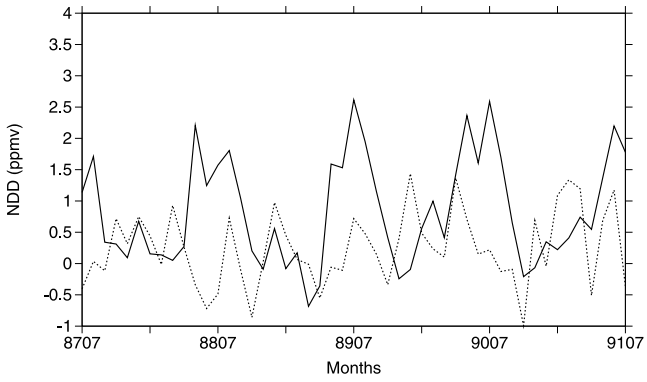


**Figure 9.** Same as Figure 8 but for South America. Dashed line is for 0°–10°N; solid line is for 0°–15°S.

than the N-DD product (Figure 10a). This is not surprising since $CO_2$ variations are influenced both by regional sources and sinks and by long-range transport acting on remote fluxes. The Northern Hemispheric seasonal cycle of $CO_2$ may, for instance, mask the effect of regional biomass burning emissions in the northern tropics (see Figures 11a and 11b over northern Africa). In contrast, the N-DD (Figures 10a and 11a) directly reflects the daily injection in the upper troposphere of $CO_2$ caused by nearby most active and extended fires. In Figure 10b we can see relatively large values of the upper air $CO_2$ concentration in October to December over South Africa, when the N-DD is close to zero. At this time of the year, fires mostly occur in Mozambique and Tanzania. In Mozambique the small values of the N-DD (less than 2 ppm in Figures 3 and 4) are probably due to prevailing wetter vegetation [*Korontzi et al.*, 2003], leading to fires less intense than in dry savannas and, consequently, less capable of injecting $CO_2$ into the upper troposphere, or to a topography less favorable to vertical transport. Tanzania is affected by important fires in November, but the absence of fires farther west weakens the mean. One additional possible reason for the enhanced $CO_2$ concentration in October to December seen in Figure 10b is the establishment of a vertical transport of $CO_2$ favored by the convection at the onset of the wet season. The fact that the N-DD signal remains close to zero would imply, for this mechanism, a diurnal cycle different from the one seen by the satellite. Similar results are obtained for South America (not shown).

[25] Other patterns of N-DD, of less than 1 ppm in magnitude, can also be seen and could reflect transport processes such as subsidence or oceanic convection, whose diurnal cycle is almost opposite to that of land convection [*Soden*, 2000] or the diurnal coupling between biospheric fluxes and vertical mixing [*Wofsy et al.*, 1988]. Signatures slightly out of this range are often associated with too small a number of days available to compute the N-DD values and may consequently be considered as less reliable. On the contrary, large N-DD values, corresponding to dry seasons with low cloudiness, are associated with a large number of days available.

## 4. Interpretation of the N-DD Signal

### 4.1. Upper Troposphere Injection and Transport of Biomass Burning $CO_2$ Plumes

[26] We explain the N-DD signal from the combination of diurnal fire-induced $CO_2$ emissions with two rapid transport

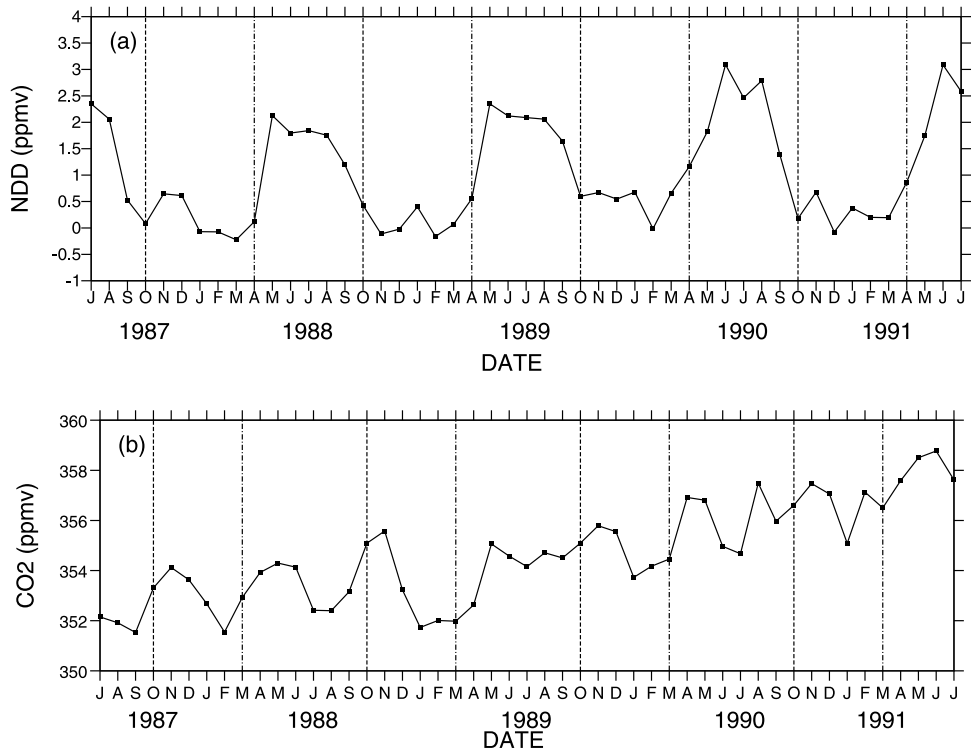


**Figure 10.** (a) Time series of the monthly mean N-DD averaged over land for southern Africa (0°–20°S). (b) Same as Figure 10a but for the monthly mean concentration of $CO_2$.

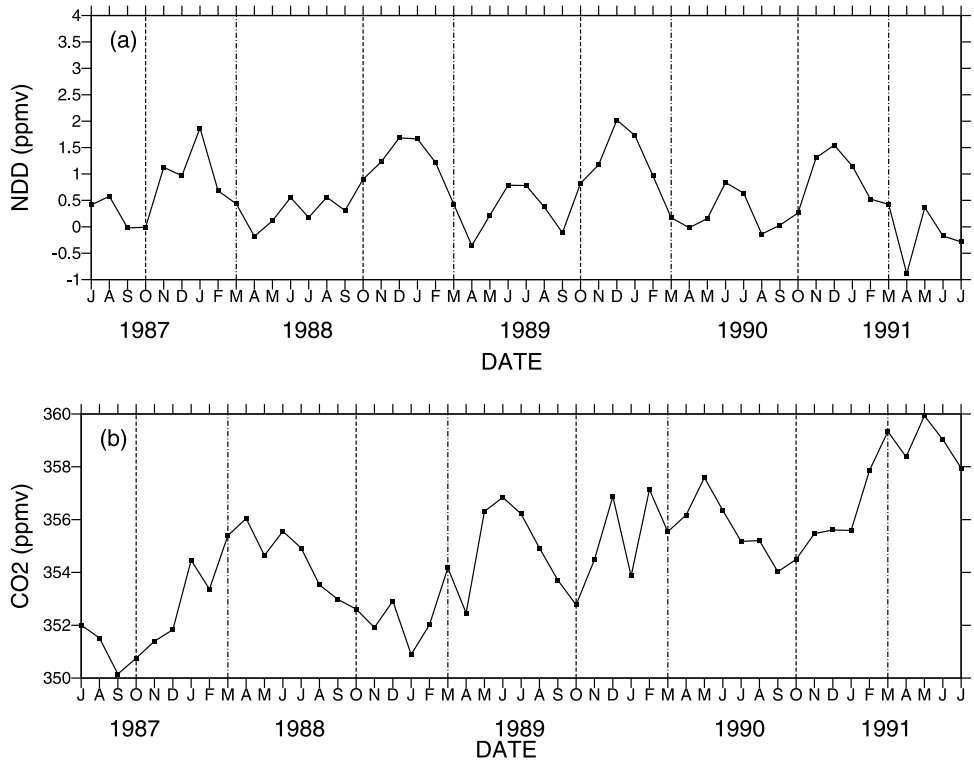


**Figure 11.** (a and b) Same as Figure 10 for northern Africa (0°–15°N).

mechanisms affecting $CO_2$ emitted by the fires. The first mechanism is a vigorous convective uplift of biomass burning plumes of $CO_2$ to the middle and upper troposphere occurring between morning and late afternoon and thus is detected by the satellite at 1930 LT. The second mechanism is a rapid (within 12 hours) dispersal of the burning emission-laden air in altitude during the night before the next satellite pass in the morning. This second mechanism of advection by the prevailing upper tropospheric flow has been studied in detail by *Krishnamurti et al.* [1996]. These authors model the transport of a tracer introduced as a sustained source in the troposphere (between 900 and 300 hPa) over the biomass burning regions of Africa and Brazil. The transport model shows rapid dispersal of the tracer at 300 hPa with a biomass burning plume emanating from Brazil and getting close to the South African coast within 1 day. *Freitas et al.* [2004] also mention that high-tropospheric plumes from South America may cross the Atlantic Ocean and reach the African continent in 1 day. This fast horizontal dispersal that occurs in the middle to high troposphere is responsible for the transport of emissions far away from the areas affected by biomass burning.

[27] The first injection mechanism is less intuitive, the apparent difficulty being, as noted by *Andreae et al.* [2001], that in the dry tropics, large-scale subsidence may prevent convection from transporting fire smoke to the upper troposphere. Yet many observations showed biomass burning plumes enriched in both CO and $O_3$ in the upper troposphere during the dry season, which could only be explained as resulting from widespread vegetation fires [*Reichle et al.*, 1990]. The EXPRESSO field campaign documented biogenic and biomass burning sources over central Africa and the exchange processes of energy and trace compounds. It was shown that at the transition between savanna and forests, vertical exchanges between the boundary layer and the upper troposphere (through the monsoon and Harmattan flows) occurred at various scales as resulting from small-scale processes (entrainment, penetrative dry convection, waves and wave breaking, boundary layer clouds, and shear wind turbulence), mesoscale processes (organized cloud coverage, local divergence-convergence fields, and penetrative cloudy convection), and synoptic-scale processes linked to subsidence and ascendance [*Delmas et al.*, 1999]. Also, subgrid-scale convective uplift of biomass burning emissions over Brazilian Amazon was modeled by *Freitas et al.* [2000] using convective kinematic trajectories. For the dry season they showed strong vertical uplift rates of up to ~8000 m above the surface within 6–8 hours, followed by advection by horizontal winds in altitude. Such combined effects of uplift and advection are corroborated by aircraft campaigns over Surinam [*Freitas et al.*, 2000; *Williams et al.*, 2001] encountering biomass burning plumes between 8 and 10 km altitude with elevated CO and $CO_2$ concentrations. In those plumes, $CO_2$ is enriched by 2–3 ppm, a signal similar in magnitude to the N-DD of Figures 2–5. *Freitas et al.* [2004] simulated fire-induced high concentration of CO in the boundary layer over South America and the vertical transport of CO to the high troposphere by convective systems associated with a cold front during the dry season. An excess of 150 ppb of CO is detrained between 9 and 13.5 km heights and is then advected by the zonal flow at an altitude of 10,700 m (250 hPa). Converted to $CO_2$ using a $CO/CO_2$ emission factor of 0.055 for savanna fires [*Andreae et al.*, 2001], this would translate into an excess

of $CO_2$ of 2.7 ppm, again in agreement with the N-DD signature.

[28] Such rapid vertical transport, however, would be sporadic during the dry season and may not explain the persistent character of the daily enhancement in upper tropospheric $CO_2$ seen in the N-DD signals. Then, fire-induced convection could be the key process that contributes to the uplifting of fire emissions. There is ample evidence that when consuming large amounts of fuel, forest fires in boreal and temperate regions can generate enough energy to create a convection column which blocks the wind at high altitudes and allows large amounts of gases and particles to reach the high atmosphere [*Lavoué et al.*, 2000; *Fromm et al.*, 2000; *Fromm and Servranckx*, 2003; *Jost et al.*, 2004; *Colarco et al.*, 2004; *Trentmann et al.*, 2004]. Recently, *Fromm et al.* [2004] claimed that fire convection should now be added to volcanoes to explain eruptive transports to the stratosphere. Within the tropics, in a recent paper, *Andreae et al.* [2004, p. 1337] report that "heavy smoke from forest fires in the Amazon was observed to reduce cloud droplet size and so delay the onset of precipitation from 1.5 kilometers above cloud base in pristine clouds to more than 5 kilometers in polluted clouds and more than 7 kilometers in pyro-clouds, the most extreme smoky clouds, feed directly on the smoke and heat from fires. Suppression of low-level rainout and aerosol washout, by invigoration of the updrafts, allows transport of water and smoke to upper levels, where the clouds appear "smoking" as they detrain much of the pollution." These authors conclude that [*Andreae et al.*, 2004, p. 1341] "the high concentrations of aerosols due to vegetation burning suppress wet removal of water and smoke, at least in the lower and middle troposphere, and thus stabilize the pollution burden. This favors the large-scale dispersal and upward transport as the dominant "sink" balancing regional pollutant emissions." This conceptual model, whose validation motivated the Large-Scale Biosphere-Atmosphere Experiment in Amazonia–Smoke, Aerosols, Clouds, Rainfall, and Climate (LBA-SMOCC), brings one possible transport mechanism able to explain the N-DD signals of Figures 2–5. It is worth recalling that the satellite observations processed here are restricted to cloud-free areas in the vicinity of the detraining clouds.

[29] Unfortunately, no systematic in situ measurements of $CO_2$ vertical profiles in the middle to upper troposphere during the peak of the fire season presently exist to validate or invalidate any of the above-proposed mechanisms (intense fire-induced dry convection, combination of dry and wet convection, etc.). *Stocks et al.* [1996], analyzing fuels and fire behaviors on savanna fires located in South Africa (around 23°S, 31°E), have indicated that savanna fires, with a limited amount of fuel available to the combustion process, cannot generate the sustained energy release levels necessary to generate convection columns above 3–4 km. However, their study was conducted in an arid savanna after a long drought period, and no definitive conclusions can be drawn before new studies on savanna fires in normal years and/or with higher fuel loads providing greater energy release rates have been undertaken. Clearly, more work remains to be done on meteorological and fire conditions necessary to affect upper tropospheric and even stratospheric injections. This includes convection column measurements from a dedicated aircraft [*Stocks et al.*, 1996].

[30] Interestingly, the fact that the N-DD maxima agree better with the model of *Hoelzemann et al.* [2004] in which seasonality comes from the GLOBSCAR product seems to indicate that the N-DD is more sensitive to large fires, from which stronger fire-induced convection may be expected, than to more numerous small (less convective) fires such as those detected by the ATSR or TRMM fire count products. This agreement reinforces the assumption of fire-induced convection as an important mechanism potentially explaining the diurnal injection of $CO_2$-laden air masses in the upper troposphere.

### 4.2. Lower Troposphere Injection of Biomass Burning $CO_2$

[31] Intense fires emit very large amounts of $CO_2$ at the surface that may also remain in the boundary layer and exchange with the lower part of the free troposphere aloft. We also checked whether a large excess of $CO_2$ at night in the lower troposphere could result in an N-DD signal consistent with the one observed. Simulations, using a large set of representative tropical situations from the TIGR climatological database [*Chédin et al.*, 2003], were carried out by increasing by 6 ppm the tropospheric $CO_2$ concentration between 0 and 7 km. The impact on the retrieved $CO_2$ was less than 0.5 ppm (altered minus original retrieval), a value (expected from the shape of the $CO_2$ Jacobian of Figure 1) too low to explain the N-DD signal. It may thus be concluded that $CO_2$-laden lower-tropospheric air has a marginal influence on the N-DD.

### 4.3. Other Factors Influencing the N-DD Signatures

[32] The magnitude of the N-DD signal is sometimes too large to be explained by $CO_2$ emissions alone. For example, in June 1990 over southern Africa we found N-DD values higher than 5 ppm locally. This raises the question of potential contaminations of the $CO_2$ retrievals by emission products other than $CO_2$. Fire emission–laden air masses uplifted to the middle to upper troposphere, if they obviously transport $CO_2$, also carry other products as aerosols, in particular smoke aerosols [*Andreae et al.*, 2004; *Koren et al.*, 2004], or ozone, often accompanying widespread fires [*Schultz et al.*, 1999; *Thompson et al.*, 2001]. Fire plumes may also transport water vapor from which upper troposphere thin cirrus clouds might eventually result, although we were unable to find studies on these matters. Because HIRS 15 μm channel radiances are sensitive to these additional absorbers, not accounted for by the retrieval scheme, their interpretation may result in erroneously large N-DD values, the load of the air mass in "foreign" products being certainly larger at 1930 LT (leading to too large a retrieved $CO_2$ column at 1930 LT) than it is at 0730 LT. The quantitative consequences of such contaminations are analyzed in detail in sections 4.3.1–4.3.3.

#### 4.3.1. Biomass Burning-Induced Aerosols

[33] The radiative impact of biomass burning aerosols in the infrared is rather poorly quantified because most optical depth measurements are within the solar part of the spectrum, either from the surface or from space observations. Therefore to assess the smoke effect on HIRS channels 2–6 requires assuming a chemical composition and size distri-

**Table 1.** Infrared (14 μm) and Visible (0.55 μm) Extinction Cross Sections ($C_{ext}$) and Their Ratios for a Set of Aerosol Components and for Three Mean Aerosol Radii[a]

| | Infrared $C_{ext}$ ($10-3$ μm$^2$) | Visible $C_{ext}$ ($10-3$ μm$^2$) | Infrared AOD/Visible AOD |
|---|---|---|---|
| | *Number Modal Diameter = 100 nm* | | |
| INSO | 0.060 | 2.69 | 0.022 |
| SOOT | 0.268 | 12.47 | 0.021 |
| WASO 50 | 0.166 | 8.55 | 0.019 |
| WASO 70 | 0.199 | 1.59 | 0.125 |
| | *Number Modal Diameter = 150 nm* | | |
| INSO | 0.203 | 17.84 | 0.011 |
| SOOT | 0.904 | 45.43 | 0.020 |
| WASO 50 | 0.56 | 30.57 | 0.018 |
| WASO 70 | 0.668 | 10.91 | 0.061 |
| | *Number Modal Diameter = 200 nm* | | |
| INSO | 0.489 | 59.7 | 0.008 |
| SOOT | 2.182 | 102.3 | 0.021 |
| WASO 50 | 1.339 | 71.9 | 0.019 |
| WASO 70 | 1.606 | 38.6 | 0.042 |

[a]AOD is aerosol optical depth; INSO is the insoluble aerosol; WASO is the water soluble aerosol, whose refractive indices depend on the relative humidity (here 50 and 70%); and SOOT describes the black carbon component.

bution for the aerosol and then computing its optical properties, in particular the extinction cross sections in the infrared (here at 14 μm) and in the visible (here at 0.55 μm), with a Mie radiative transfer code. The infrared optical depth is then obtained by multiplying the calculated infrared to visible optical depth ratio by the observed visible optical depth. This ratio has been calculated for a set of primary aerosol types and particle mean radius. The primary aerosol model refractive indices are taken from the Optical Properties of Aerosol and Clouds database [*Hess et al.*, 1998]. INSO is the insoluble aerosol. WASO is the water soluble aerosol, whose refractive indices strongly depend on the relative humidity. Here we have considered two values: 50 and 70%, as dry season fire-induced aerosol occurs for relative humidity below 70% [*Reid et al.*, 2004]. SOOT describes the black carbon component. Extinction cross sections have been computed for three values of the aerosol mean radius: 100, 150, and 200 nm according to recent in situ observations reported by *Andreae et al.* [2004]. As shown in Table 1, the infrared to visible optical depth ratio strongly varies with the aerosol type and size, from about 0.008 to 0.12. In reality, however, smoke aerosol is a mixture of the different primary aerosol components of Table 1. For a realistic mixture [*Reid et al.*, 2004] the maximum infrared to visible optical depth ratio comes to 0.07. It is worth noting that whatever the aerosol type is, because the size parameter is small, the single scattering albedo is below 0.01 at 14 μm, and so only absorption needs to be considered. Consequently, the impact of smoke on the HIRS 2 channels only depends on the optical depth and vertical distribution of the aerosol.

[34] Using MODIS global aerosol products (available at http://modis-atmos.gsfc.nasa.gov/MOD08_M3/index.html), we first looked for the highest observed $15° \times 15°$ monthly mean visible aerosol optical depth (AOD) value. A maximum of 0.7 was found over South Africa in August 2003. Note that by definition this AOD integrates the whole atmospheric column, from the surface to the top of the atmosphere. With the above infrared to visible ratio of 0.07 this value corresponds to a maximum infrared aerosol optical depth of 0.05. Sensitivity tests were then carried out by varying infrared optical depths from 0.005 to 0.05 at 14 μm and aerosol layer altitudes from the surface to 7 km using a large set (872) of representative tropical atmospheres from the TIGR database. Channels 2, 3, and 4 showed no sensitivity to aerosols while channel 5 sensitivity was about half that of channel 6. In contrast, any given variation of the $CO_2$ column concentration has approximately the same effect on these two channels. The lack of coherence of the aerosol signal relative to the $CO_2$ signal explains why about half of the aerosol signal translates into an increased noise (from 0.1 to 2 ppm, depending on the aerosol optical depth and altitude), while the second half results in a bias in the $CO_2$ concentration. This bias is shown as a function of smoke height and optical depth in Figure 12. The sign of the bias (aerosol loaded minus clear atmospheric path) comes from the fact that about one half of the absorption caused by the aerosol is erroneously attributed to $CO_2$. Figure 12 shows the large impact of the altitude of the smoke: A bias caused by a smoke layer located at 6 km is ~5 times greater than a bias caused by the same layer located at 3 km. Observations show that biomass burning aerosols with a radiative impact in the infrared (large particle sizes) stay relatively low in the troposphere [e.g., *Anderson et al.*, 1996], which would greatly reduce the contamination of the HIRS channels, peaking above 800 hPa, used here to retrieve $CO_2$ columns. Recent studies suggest that dense smoke might be found at higher altitudes [*Andreae et al.*, 2004], but no in situ observations of aerosol concentration and size in the upper troposphere have been done yet. However, even in the latter situation, there is still a substantial amount of the aerosol which stays in the lower troposphere. Therefore only a smaller part of the total optical depth should be attributed to high-altitude particles. Moreover, assuming, like *Andreae et al.* [2001], that the large majority of the accumulation mode particles are removed during convection suggests an infrared optical depth for the high-altitude aerosols of the order of 0.01 or less, corresponding to a maximum bias in the

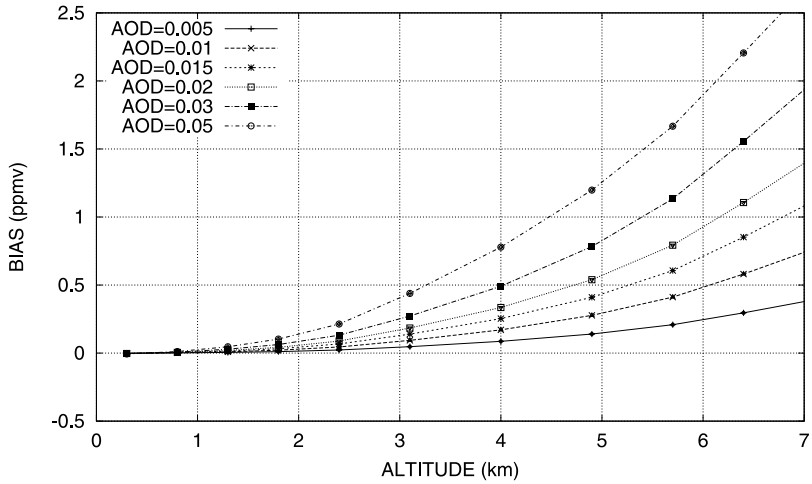


**Figure 12.** Simulations, based on Table 1 results, of $CO_2$ concentration biases (in ppm) caused by absorbing aerosols, as a function of the aerosol layer altitude (0–7 km) and optical depth (AOD) at 14 μm (0.005–0.05). As explained in the text, simulations with high optical depths at high altitudes are not realistic. It is most likely that realistic values of the fire-induced $CO_2$ concentration biases are of the order of 1 ppm or less. This does not exclude paroxysmal events with significantly larger biases.

N-DD due to smoke aerosols of the order of 1 ppm or less.

#### 4.3.2. Biomass Burning–Induced Ozone

[35] The HIRS 15 μm channels are sensitive to ozone but much less than to $CO_2$ [*Chédin et al.*, 2002]. For example, a variation of 1% of the $CO_2$ column and a variation of 10% of the ozone column (mostly driven by its stratospheric part) would produce a change of 0.1 K in the brightness temperature of channel 5 (the most sensitive to $CO_2$, with channel 6). A much smaller variation of 0.02 K is obtained if only the tropospheric ozone column (surface to 130 hPa) is varied by the same amount of 10%. Moreover, these variations induced by tropospheric ozone are not in phase, channel by channel, with those induced by a variation of $CO_2$, contributing to disentangling the two sources of variations. For that reason, $O_3$ variations are only partly causing a bias, the rest being interpreted as noise. To simulate tropospheric ozone concentration variations induced by fires (their influence on the stratospheric column is negligible), we conservatively took 100 ppb as an upper bound value for ozone-enriched plumes [*Jonquieres et al.*, 1998]. To quantify the aliasing effect of an increase of ozone on the $CO_2$ retrievals, the set of representative tropical atmospheric situations from TIGR was altered by arbitrarily doubling the tropospheric $O_3$ column (1013–130 hPa), leading to a mean value of 100 ppb (from an original value around 50 ppb), with a standard deviation of ~25 ppb, in agreement with the highest $O_3$ values observed. The impact on N-DD was a bias of 1.0 ppm (altered minus original retrieval), with a standard deviation of 0.40 ppm. Another potential disturbance by ozone variations may come from intrusions of stratospheric air with an elevated concentration of $O_3$ [*Waugh and Polvani*, 2000] into the troposphere. However, not being diurnal, such signals which might affect the monthly $CO_2$ product do not affect the N-DD signal.

#### 4.3.3. Fire-Induced Very Thin Cirrus

[36] Very thin cirrus, often understood as clouds with a visible optical depth of less than 0.03, a value of the order of the limit of detection of our cloud screening scheme (~0.05, resulting from simulations using typical thin cirrus microphysical properties [*Luo et al.*, 2003]), have often been observed near the tropical tropopause. They occur predominantly over the convectively active regions of the western Pacific, South America, or Africa but can also be observed far from potential convective sources. They extend several hundreds to more than a thousand kilometers and persist for time periods of several hours to about a day before dissipating [*Winker and Trepte*, 1998; *Hartmann et al.*, 2001]. As explained by *Chédin et al.* [2003], because it may reasonably be expected that most of the radiance contamination from such clouds is largely diluted by the space (15°) and time (1 month) averaging used to produce mean $CO_2$ concentrations, only long-lasting and extended, or systematic, episodes of contamination by undetected very thin cirrus, quite unlikely to happen according to present observations, could result in erroneous retrievals of the concentration of $CO_2$.

[37] We were unable to find observations or studies reporting on the association of thin tropopause cirrus and biomass burning. Two quite speculative assumptions are indeed required to envisage the formation of such fire-induced thin cirrus and their potential impact on the N-DD signal: (1) Water vapor accompanying biomass burning emissions must be injected at the mean altitude of the tropical tropopause (17–18 km), roughly double that required to explain the $CO_2$ N-DD signal, and (2) they must be present at the time of the peak of fire activity (1930 LT) and have disappeared 12 hours later (0730 LT), systematically. We did not consider this scenario as being realistic and concluded that such a source of contamination of the N-DD signal would be quite unlikely.

## 5. Discussion

[38] From the study in section 4.3 we conclude that the principal source of contamination of the N-DD signal by fire-induced products other than $CO_2$ comes from high-

altitude and large infrared optical depth aerosols. In contrast, low-altitude aerosol cannot explain the highest N-DD values (Figure 12). High-altitude aerosol with (unrealistic?) high optical depths may, on the contrary, contribute to the enhancement of the N-DD signal which could then be overinterpreted in terms of $CO_2$. Ozone may also enhance the N-DD signal, however, by no more than 1 ppm. Our sensitivity study of the contamination by non-$CO_2$ absorbers raises a caution flag on a quantitative use of the N-DD product, for instance, in inversion studies. It is nevertheless important in the sense that it supports the mechanism of fire-induced plumes of $CO_2$ and other emission products being vigorously uplifted into the upper troposphere during daytime and dispersed at night by large-scale atmospheric transport. Up until the effects of non-$CO_2$ absorbers can be deconvoluted from the $CO_2$ signal, we believe that the N-DD signal is more an indicator of the intensity and location of the fires and of the injection of their emissions at high altitude than a quantitative measure of the amount of $CO_2$ brought to the upper troposphere by the fires. Because we expect a high correlation between CO and $CO_2$ in biomass burning emissions, vertically resolved global measurements of the CO distribution in the troposphere from the MOPITT instrument could bring important information on the role of biomass burning in the injection of emission products high in the troposphere. However, crossing the equator at 1030 and 2230 LT, instead of 0730 LT for TOVS, the MOPITT observations may bracket the peak of the fire activity either too early or too late for capturing the maximum of the difference between nighttime and daytime concentrations.

## 6. Conclusion

[39] This new satellite retrieval of upper tropospheric column of $CO_2$, at 0730 and 1930 LT in the tropics, shows unsuspected patterns in regions where almost no in situ measurements exist. The most striking feature is a strong increase in the night (1930 LT) minus day (0730 LT) difference of the retrieved $CO_2$ column over areas affected by intense fires. Both the seasonal and the interannual variability of this $CO_2$ difference follow the most recent studies on space and time distribution of fires. In particular, the agreement with the European Space Agency's monthly Global Burnt Scar (GLOBSCAR) product, which is recognized as yielding reasonable estimates of burned areas for larger and presumably more intense fires, is remarkable. It seems to indicate that the N-DD signature responds more to the burned area, and presumably to the intensity of fire-induced convection, than to the number of fires. Such a diurnal signal could be explained by vigorous fire-induced vertical uplift of biomass burning plumes from the surface to the upper troposphere, following a conceptual model recently proposed by *Andreae et al.* [2004], coupled to rapid dispersal of emission-laden air masses by the horizontal flow in altitude. However, the magnitudes of a few extreme N-DD values (e.g., over Africa in August 1990 of the order of more than 5 ppm locally), seem to point out a potential significant contamination of the N-DD signal by fire emission products other than $CO_2$. It is concluded from a detailed sensitivity analysis that the main potential source of contamination may come from high-altitude aerosols with a large infrared optical depth. Such an occurrence can only be explained by a vigorous injection of biomass burning emission products in the high troposphere and would render the N-DD signal more an indicator of the intensity and location of the fires than a measure of the injection of $CO_2$ in the upper troposphere.

[40] Further analysis includes the processing of the whole NOAA-TOVS series from 1979 to the present and of the Atmospheric Infrared Sounder (AIRS) now flying aboard the satellite Aqua/NASA and for which the method developed for TOVS has been recently adapted [*Crevoisier et al.*, 2004] as well as the assimilation of such data in atmospheric $CO_2$ flux inversions. Preliminary simulations using the general circulation model LMD-Z (F. Hourdin, private communication, 2004) should also be started to further analyze the injection of biomass burning emissions into the upper troposphere. Following *Stocks et al.* [1996], further studies would highly benefit from a dedicated campaign of in situ measurements (surface and aircraft) conducted in both subhumid and humid savannas in order to further assess the behavior of fire-induced convection and corresponding injection heights.

[41] **Acknowledgments.** We are happy to thank R. Armante, F. M. Bréon, F. Chevallier, and P. Peylin for their help, fruitful discussions, and constructive criticisms. This work has been supported in part by the European Community under the contract (''COCO'') EVG1-CT-2001-00056. Warm thanks are also due to the two anonymous referees for their constructive and helpful comments and criticism.

## References

Anderson, B. E., et al. (1996), Aerosols from biomass burning over the tropical South Atlantic region: Distribution and impacts, *J. Geophys. Res.*, *101*, 24,117–24,137.

Andreae, M. O. (1996), *Fire in the Southern African Savanna: Ecological and Environmental Perspectives*, edited by B. W. van Wilgen et al., pp. 161–183, Witwaterstrand Univ. Press, Johannesburg, South Africa.

Andreae, M. O., et al. (2001), Transport of biomass burning smoke to the upper troposphere by deep convection in the equatorial region, *Geophys. Res. Lett.*, *28*, 951–954.

Andreae, M. O., D. Rosenfeld, P. Artaxo, A. A. Costa, G. P. Frank, K. M. Longo, and M. A. F. Silva Dias (2004), Smoking rain clouds over the Amazon, *Science*, *303*, 1337–1342.

Arino, O., and J. M. Mellinote (1995), Fire atlas index, *Earth Obs. Q.*, *50*, 11–16.

Arino, O., and S. Plummer (2001), The along-track scanning radiometer World Fire Atlas detection of night-time fire activity, validation report, *IGBP-DIS Working Pap. 23*, Int. Geosphere Biosphere Programme, Stockholm.

Barbosa, P. M., J. M. Grégoire, and J. M. C. Pereira (1997), Detection of burned areas in Africa using a multitemporal multithreshold analysis of NOAA-AVHRR-GAC data, in *Earth Surface Remote Sensing*, edited by G. Cecchi et al., *Proc. SPIE Int. Soc. Opt. Eng.*, *3222*, 67–75.

Barbosa, P. M., D. Stroppiana, J. M. Grégoire, and J. M. C. Pereira (1999), An assessment of vegetation fire in Africa (1981–1991): Burned areas, burned biomass, and atmospheric emissions, *Global Biogeochem. Cycles*, *13*, 933–950.

Cahoon, D. R., B. J. Stocks, J. S. Levine, W. R. Coter III, and C. P. O'Neill (1992), Seasonal distribution of African savanna fires, *Nature*, *359*, 812–815.

Chatfield, R. B., Z. Guo, G. W. Sachse, D. R. Blake, and N. J. Blake (2002), The subtropical global plume in the Pacific Exploratory Mission-Tropics A (PEM-Tropics A), PEM-Tropics B, and the Global Atmospheric Sampling Program (GASP): How tropical emissions affect the remote Pacific, *J. Geophys. Res.*, *107*(D16), 4278, doi:10.1029/2001JD000497.

Chédin, A., N. A. Scott, C. Wahiche, and P. Moulinier (1985), The improved initialization inversion method: A high resolution physical method for temperature retrievals from satellites of the TIROS-N series, *J. Clim. Appl. Meteorol.*, *24*, 128–143.

Chédin, A., S. Serrar, R. Armante, N. A. Scott, and A. Hollingsworth (2002), Signatures of annual and seasonal variations of $CO_2$ and other

greenhouse gases from NOAA/TOVS observations and model simulations, *J. Clim.*, *15*, 95–116.
Chédin, A., S. Serrar, N. A. Scott, C. Crevoisier, and R. Armante (2003), First global measurement of midtropospheric $CO_2$ from NOAA polar satellites: Tropical zone, *J. Geophys. Res.*, *108*(D18), 4581, doi:10.1029/2003JD003439.
Chevallier, F., F. Cheruy, N. A. Scott, and A. Chédin (1998), A neural network approach for a fast and accurate computation of a longwave radiative budget, *J. Appl. Meteorol.*, *37*, 1385–1397.
Colarco, P. R., M. R. Schoeberl, B. G. Doddridge, L. T. Marufu, O. Torres, and E. J. Welton (2004), Transport of smoke from Canadian forest fires to the surface near Washington, D. C.: Injection height, entrainment, and optical properties, *J. Geophys. Res.*, *109*, D06203, doi:10.1029/2003JD004248.
Cooke, W., B. Koffi, and J.-M. Gregoire (1996), Seasonality of vegetation fires in Africa from remote sensing data and application to a global chemistry model, *J. Geophys. Res.*, *101*, 21,051–21,065.
Crevoisier, C., S. Heilliette, A. Chédin, S. Serrar, R. Armante, and N. A. Scott (2004), Midtropospheric $CO_2$ concentration retrieval from AIRS observations in the tropics, *Geophys. Res. Lett.*, *31*, L17106, doi:10.1029/2004GL020141.
Crutzen, P. J., and M. O. Andreae (1990), Biomass burning in the tropics: Impact on atmospheric chemistry and biogeochemical cycles, *Science*, *250*, 1678–1699.
Delmas, R. A., et al. (1999), Experiment for Regional Sources and Sinks of Oxidants (EXPRESSO): An overview, *J. Geophys. Res.*, *104*, 30,609–30,624.
Duncan, B. N., R. V. Martin, A. C. Staudt, R. Yevich, and J. A. Logan (2003), Interannual and seasonal variability of biomass burning emissions constrained by satellite observations, *J. Geophys. Res.*, *108*(D2), 4100, doi:10.1029/2002JD002378.
Fishman, J., J. M. Hoell, R. D. Bendura, R. J. McNeil, and V. W. J. H. Kirchhoff (1996), NASA GTE TRACE A Experiment (September-October 1992): Overview, *J. Geophys. Res.*, *101*, 23,865–23,880.
Freitas, S. R., M. A. F. Silva Dias, and P. L. A. Silva Dias (2000), A convective kinematic trajectory technique for low-resolution atmospheric models, *J. Geophys Res.*, *105*, 24,375–24,386.
Freitas, S. R., K. M. Longo, M. A. F. Silva Dias, P. L. Silva Dias, R. Chatfield, E. Prins, P. Artaxo, G. A. Grell, and F. S. Recuero (2004), Monitoring the transport of biomass burning emissions in South America, *Environ. Fluid Mech.*, *5*, 135–167.
Fromm, M., and R. Servranckx (2003), Transport of forest fire smoke above the tropopause by supercell convection, *Geophys. Res. Lett.*, *30*(10), 1542, doi:10.1029/2002GL016820.
Fromm, M., J. Alfred, K. Hoppel, J. Hornstein, R. Bevilacqua, E. Shettle, R. Sevranckx, Z. Li, and B. Stocks (2000), Observations of boreal forest fire smoke in the stratosphere by POAM III, SAGE II, and lidar in 1998, *Geophys. Res. Lett.*, *27*, 1407–1410.
Fromm, M., R. Bevilacqua, B. Stocks, and R. Servranckx (2004), New directions: Eruptive transport to the stratosphere—Add fire-convection to volcanoes, *Atmos. Environ.*, *38*, 163–165.
Giglio, L., J. D. Kendall, and R. Mack (2003), A multi-year active fire data set for the tropics derived from the TRMM VIRS, *Int. J. Remote Sens.*, *24*, 4505–4525.
Hao, W. M., and M. H. Liu (1994), Spatial and temporal distribution of tropical biomass burning, *Global Biogeochem. Cycles*, *8*, 495–503.
Hartmann, D. L., J. R. Holton, and Q. Fu (2001), The heat balance of the tropical tropopause, cirrus, and stratospheric dehydration, *Geophys. Res. Lett.*, *28*, 1969–1972.
Hauglustaine, D. A., G. P. Brasseur, S. Walters, P. J. Rasch, J.-F. Müller, L. K. Emmons, and M. A. Carroll (1998), MOZART, a global chemical transport model for ozone and related chemical tracers: 2. Model results and evaluation, *J. Geophys. Res.*, *103*, 28,291–28,335.
Hess, M., P. Koepke, and I. Schult (1998), Optical properties of aerosols and clouds: The software package OPAC, *Bull. Am. Meteorol. Soc.*, *79*, 831–844.
Hoelzemann, J. J., M. G. Schultz, G. P. Brasseur, C. Granier, and M. Simon (2004), Global wildland fire emission model GWEM: Evaluating the use of global area burnt satellite data, *J. Geophys. Res.*, *109*, D14S04, doi:10.1029/2003JD003666.
Houweling, S., F.-M. Breon, I. Aben, C. Rodenbeck, M. Gloor, M. Heimann, and P. Ciais (2003), Inverse modeling of $CO_2$ sources and sinks using satellite data: A synthetic intercomparison of measurement techniques and their performances as a function of space and time, *Atmos. Chem. Phys.*, *4*, 523–538.
Hsu, N. C., J. R. Herman, P. K. Bhartia, C. J. Seftor, O. Torres, A. M. Thompson, J. F. Gleason, T. F. Eck, and B. N. Olben (1996), Detection of biomass burning smoke from TOMS measurements, *Geophys. Res. Lett.*, *23*, 745–748.
Jonquieres, I., A. Marenco, and A. Maalej (1998), Study of ozone formation and transatlantic transport from biomass burning emissions over West Africa during the airborne Tropospheric Ozone campaigns TROPOZ I and TROPOZ II, *J. Geophys. Res.*, *103*, 19,059–19,073.
Jost, H.-J., et al. (2004), In-situ observations of mid-latitude forest fire plumes deep in the stratosphere, *Geophys. Res. Lett.*, *31*, L11101, doi:10.1029/2003GL019253.
Kasischke, E. S., and J. E. Penner (2004), Improving global estimates of atmospheric emissions from biomass burning, *J. Geophys. Res.*, *109*, D14S01, doi:10.1029/2004JD004972.
Koren, I., Y. J. Kaufman, L. A. Remer, and J. V. Martins (2004), Measurement of the effect of Amazon smoke on inhibition of cloud formation, *Science*, *303*, 1342–1345.
Korontzi, S., C. O. Justice, and R. J. Scholes (2003), Influence of timing and spatial extent of savanna fires in southern Africa on atmospheric emissions, *J. Arid Environ.*, *54*, 395–404.
Krishnamurti, T. N., M. C. Sinha, M. Kanamitsu, D. Oosterhof, H. E. Fuelberg, R. Chatfield, D. J. Jacob, and J. Logan (1996), Passive tracer transport relevant to the TRACE A experiment, *J. Geophys. Res.*, *101*, 23,889–23,907.
Langaas, S. (1993), Diurnal cycles in savanna fires, *Nature*, *363*, 120.
Langenfelds, R. L., R. J. Francey, B. C. Pak, L. P. Steele, J. Lloyd, C. M. Trudinger, and C. E. Allison (2002), Interannual growth rate variations of atmospheric $CO_2$ and its $\delta^{13}C$, $H_2$, $CH_4$, and CO between 1992 and 1999 linked to biomass burning, *Global Biogeochem. Cycles*, *16*(3), 1048, doi:10.1029/2001GB001466.
Lavoué, D., C. Liousse, and H. Cachier (2000), Modeling of carbonaceous particles emitted by boreal and temperate wildfires at northern latitudes, *J. Geophys. Res.*, *105*, 26,871–26,890.
Lindesay, J. A., M. O. Andreae, J. G. Goldammer, G. Harris, H. J. Annegarn, M. Garstang, R. J. Scholes, and B. W. Van Wilgen (1996), International Geosphere-Biosphere Programme/International Global Atmospheric Chemistry SAFARI 92 field experiment: Background and overview, *J. Geophys. Res.*, *101*, 23,521–23,530.
Luo, B. P., et al. (2003), Dehydration potential of ultrathin clouds at the tropical tropopause, *Geophys. Res. Lett.*, *30*(11), 1557, doi:10.1029/2002GL016737.
Matsueda, H., H. Y. Inoue, and M. Ishii (2002), Aircraft observation of carbon dioxide at 8–13 km altitude over the western Pacific from 1993 to 1999, *Tellus, Ser. B*, *54*, 1–21.
Prins, E. M., and W. P. Menzel (1992), Geostationary satellite detection of biomass burning in South America, *Int. J. Remote Sens.*, *13*, 2783–2799.
Prins, E. M., J. M. Feltz, W. P. Menzel, and D. E. Ward (1998), An overview of GOES 8 diurnal fire and smoke results for SCAR-B and 1995 fire season in South America, *J. Geophys. Res.*, *103*, 31,821–31,835.
Reichle, H. G., V. S. Connors, J. A. Holland, W. D. Hypes, H. A. Wallio, J. C. Casas, B. B. Gormsen, M. S. Saylor, and W. D. Hesketh (1990), The distribution of middle tropospheric carbon monoxide during early October 1984, *J. Geophys. Res.*, *95*, 9845–9856.
Reid, J. S., R. Koppmann, T. F. Eck, and D. P. Eleuterio (2004), A review of biomass burning emissions, part II: Intensive physical properties of biomass burning particles, *Atmos. Chem. Phys. Disc.*, *4*, 5135–5200.
Rodenbeck, C., S. Houweling, M. Gloor, and M. Heimann (2003), $CO_2$ flux history 1982–2001 inferred from atmospheric data using a global inversion of atmospheric transport, *Atmos. Chem. Phys.*, *3*, 1919–1964.
Rumelhart, D. E., G. E. Hinton, and R. J. Williams (1986), *Parallel Distributed Processing: Explorations in the Macrostructure of Cognition*, edited by D. E. Rumelhart and J. L. McClelland, pp. 318–362, MIT Press, Cambridge, Mass.
Schimel, D., and D. Baker (2002), The wild fire factor, *Nature*, *420*, 29–30.
Schultz, M. G. (2002), On the use of ATSR fire count data to estimate the seasonal and interannual variability of vegetation fire emissions, *Atmos. Chem. Phys.*, *2*, 387–395.
Schultz, M. G., et al. (1999), On the origin of tropospheric ozone and $NO_x$ over the tropical South Pacific, *J. Geophys. Res.*, *104*, 5829–5843.
Seiler, W., and P. J. Crutzen (1980), Estimates of gross and net fluxes of carbon between the biosphere and the atmosphere from biomass burning, *Clim. Change*, *2*, 207–247.
Siegert, F., G. Ruecker, A. Hinrichs, and A. A. Hoffmann (2001), Increased damage from fires in logged forests during droughts caused by El Nino, *Nature*, *414*, 437–440.
Simon, M., S. Plummer, F. Fierens, J. J. Hoelzemann, and O. Arino (2004), Burnt area detection at global scale using ATSR-2: The GLOBSCAR products and their qualification, *J. Geophys. Res.*, *109*, D14S02, doi:10.1029/2003JD003622.
Smith, W. L., H. M. Woolf, C. M. Hayden, D. Q. Wark, and L. M. McMillin (1979), The TIROS-N Operational Vertical Sounder, *Bull. Am. Meteorol. Soc.*, *60*, 1177–1187.

Soden, B. J. (2000), The diurnal cycle of convection, clouds and water vapour in the tropical upper troposphere, *Geophys. Res. Lett.*, *27*, 2173–2176.

Stocks, B. J., B. W. van Wilgen, W. S. W. Troloppe, D. J. McRae, J. A. Mason, F. Weirich, and A. L. F. Potgieter (1996), Fuels and fire behavior dynamics on large-scale savanna fires in Kruger National Park, South Africa, *J. Geophys. Res.*, *101*, 23,541–23,550.

Stohl, A., S. Eckhardt, C. Forster, P. James, and N. Spitchtinger (2002), On the pathways and timescales of intercontinental air pollution transport, *J. Geophys. Res.*, *107*(D23), 4684, doi:10.1029/2001JD001396.

Thompson, A. M., J. C. Witte, R. D. Hudson, H. Guo, J. R. Herman, and M. Fujiwara (2001), Tropical tropospheric ozone and biomass burning, *Science*, *291*, 2128–2132.

Trentmann, J., T. Winterrath, G. Luderer, C. Textor, M. D. Fromm, R. Servranckx, D. Rosenfeld, P. K. Wang, P. V. Hobbs, and M. O. Andreae (2004), Formation of a fire-induced convective cloud: A model study of the Chisholm fire, 28 May 2001, paper presented at 14th International Conference on Clouds and Precipitation, Int. Comm. on Clouds and Precip. of the Int. Assoc. of Meteorol. and Atmos. Sci., Bologna, Italy.

van der Werf, G. R., J. T. Randerson, G. J. Collatz, and L. Giglio (2003), Carbon emissions from fires in tropical and subtropical ecosystems, *Global Change Biol.*, *9*, 547–562.

van der Werf, G. R., J. T. Randerson, G. J. Collatz, L. Giglio, P. S. Kasibhatla, A. F. Arellano Jr., S. C. Olsen, and E. S. Kasischke (2004), Continental partitioning of fire emissions during the 1997 to 2001 El Niño/La Niña period, *Science*, *303*, 73–76.

Waugh, D. W., and L. M. Polvani (2000), Climatology of intrusions into the tropical upper troposphere, *Geophys. Res. Lett.*, *23*, 3857–3860.

Williams, J., H. Fischer, P. Hoor, U. Pöschl, P. J. Crutzen, M. O. Andreae, and J. Lelieveld (2001), The influence of the tropical rainforest on atmospheric CO and $CO_2$ as measured by aircraft over Surinam, South America, *Chemosphere Global Change Sci.*, *3*, 157–170.

Winker, D. M., and C. R. Trepte (1998), Laminar cirrus observed near the tropical tropopause by LITE, *Geophys. Res. Lett.*, *25*, 3351–3354.

Wittenberg, U., M. Heimann, G. Esser, A. David McGuire, and W. Sauf (1998), On the influence of biomass burning on the seasonal $CO_2$ signal as observed at monitoring stations, *Global Biogeochem. Cycles*, *12*, 531–544.

Wofsy, S. C., R. C. Harris, and W. A. Kaplan (1988), Carbon dioxide in the atmosphere over the Amazon basin, *J. Geophys. Res.*, *93*, 1377–1387.

A. Chédin, C. Pierangelo, N. A. Scott, and S. Serrar, Laboratoire de Météorologie Dynamique, IPSL, Ecole Polytechnique, F-91128 Palaiseau Cedex, France. (chedin@lmd.polytechnique.fr)

P. Ciais, Laboratoire des Sciences du Climat et de l'Environnement, CEA/IPSL, l'Orme des Merisiers, F-91191 Gif-sur-Yvette, France.